SEMARAK ILMU PUBLISHING

Journal of Advanced Research in Fluid Mechanics and Thermal Sciences

Journal homepage:
https://semarakilmu.com.my/journals/index.php/fluid_mechanics_thermal_sciences/index
ISSN: 2289-7879

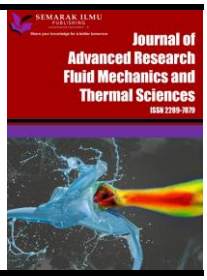

Enhancing Convective Heat Transfer in Circular Microchannels through Response Surface Methodology of Orifice Geometry: A Computational Fluid Dynamics Approach

Dimas Agung Putra Harsono[1], Dieter Rahmadiawan[2,3], Ridho Irwansyah[1,*]

[1] Department of Mechanical Engineering, Faculty of Engineering, Universitas Indonesia, 16424 Depok, Indonesia
[2] Department of Mechanical Engineering, National Cheng Kung University (NCKU), Tainan, Taiwan
[3] Department of Mechanical Engineering, Universitas Negeri Padang, 25173, Padang, Sumatera Barat, Indonesia

ARTICLE INFO

Article history:
Received 7 July 2024
Received in revised form 22 October 2024
Accepted 3 November 2024
Available online 20 November 2024

Keywords:
Microchannel; Orifice; Reynolds number; heat flux; pressure drop; Nusselt number; response surface methodology

ABSTRACT

This research investigates the use of Computational Fluid Dynamics (CFD) simulation to model circular microchannel pipes with orifices as a passive heat transfer enhancer. Different parameters, including microchannel geometry, Reynolds number, and heat flux, are employed in this research. The analysis results indicate that factors such as the distance between the inlet and orifice, and Reynolds number significantly influence the system performance, particularly in terms of pressure drop and Nusselt number. The addition of an orifice to a microchannel also affects the efficiency of heat transfer and the pressure drop. The results were further analysed using the Response Surface Methodology, which revealed that a microchannel with a Reynolds number of 90 and a distance between the inlet and orifice of 2.83238 mm provides an optimum solution. In conclusion, optimising these parameters can lead to more efficient and optimal designs for microfluidic applications.

1. Introduction

The advancement of technology, particularly in the field of electronics, has led to a reduction in component size accompanied by an increase in the density of electronic components per unit area. Consequently, the risk of the operating temperature of electronic components exceeding allowable limits has increased. The inability to dissipate heat quickly can lead to performance degradation or even the premature failure of electronic components [1]. A variety of strategies have been employed to enhance heat transfer efficiency in a range of applications, including chemical processes, cooling, heat exchangers, and automotive cooling systems. This approach involves the implementation of enhancement techniques with the objective of improving performance, reducing dimensions, and optimising operational costs. Heat transfer enhancement methods can be classified into two main categories: passive methods, which include turbulence generation through geometric modifications,

* *Corresponding author.*
E-mail address: ridho.irwansyah04@ui.ac.id

https://doi.org/10.37934/arfmts.124.1.93110

such as twisted tape, tangential inlet nozzles, spiral fins, and others. In contrast, active methods involve the addition of external energy, such as an increase in pumping power.

Heat exchangers are highly efficient systems for transferring large amounts of heat due to their larger surface area [2]. The dimensions of channels in heat exchangers are becoming increasingly compact, a phenomenon known as microchannels. The advantages of microchannels include a reduction in weight and the use of less material [3]. Various studies have investigated the geometry of microchannels. Wu and Little [4] examined rectangular microchannels and discovered that the Nusselt number varies with the Reynolds number in laminar flow. They also found that the Nusselt number of microchannels was higher than that of conventional heat exchangers. Dehghan *et al.,* [5] employed straight microchannel heat sinks and observed that the Nusselt number increased in tandem with the convective heat transfer coefficient. Furthermore, Kose *et al.,* [6] demonstrated that the aspect ratio of rectangular microchannels is related to the heat transfer area and that this configuration is more effective than trapezoidal microchannels. Wang *et al.,* [7] conducted a numerical study to investigate the impact of microchannel cross-section on heat transfer performance. Their numerical predictions indicated that the rectangular section exhibited the highest thermal performance, while the triangular section exhibited the lowest thermal performance among the three shapes. Their numerical predictions showed that the rectangular section provided the highest thermal performance, while the triangular section provided the lowest thermal performance among the three shapes.

Kim [8] conducted an experimental investigation of straight microchannels with aspect ratios ranging from 0.25 to 3.8, with a view to comparing theoretical and experimental values of the Nusselt number. In a double-pipe heat exchanger, Murugasen *et al.,* [9] experimentally examined heat transfer using square-cut twisted tapes (STT) and plain twisted tapes (PTT) with variations in twist ratio. The results indicated that the Nusselt number increased by 14% in the system using plain twisted tapes (PTT). He *et al.,* [10] documented the effect of helically twisted tape on the friction factor and on the heat transfer of cross-flow air heaters. Their study confirmed that swirl flow enhances heat transfer compared to pure axial flow, with the cost of pressure drop in the resulting turbulent flow. Ali *et al.,* [11] studied the performance of straight tape and twisted tape in circular cross-section microchannels. They found that at a Reynolds number of 350, the microchannel with twisted tape exhibited superior thermal performance. The Nusselt number of the microchannel with twisted tape was 40% higher than that of the microchannel without twisted tape, while its thermal resistance was 37% lower than that of the microchannel without twisted tape.

Song *et al.,* [12] employed twisted tapes in microchannels, resulting in a 24% increase in the average Nusselt number, a 50% increase in flow drag, and a maximum comprehensive thermal performance of 1.55. Furthermore, Eiamsa-Ard *et al.,* [13] examined the exchange between heat transfer gain and pressure drop from the use of one to three twisted tapes in a cork pattern in a pipe. Their experiments demonstrated that a single twisted tape filament in a cork pattern provides the optimal trade-off between heat transfer enhancement and pressure drop. Vinoth *et al.,* [14] examined the heat and flow characteristics of different microchannel geometries and found that curved microchannels yielded superior results. The heat transfer and pressure drop increased by 11.98% and 30.1%, respectively, when compared to straight microchannels. Furthermore, Dhamane *et al.,* [15] examined plain tubes with wavy twisted tapes with wave widths of 13, 16, and 24 mm at a constant wall heat flux and different mass flow rates. The highest Nusselt number was observed for wavy twisted tapes with wave widths of 13 mm. The percentage increase in Nusselt number for wavy twisted tapes in comparison to plain tubes ranged from 32 to 98%, 31 to 89%, and 26 to 87% for tapes with a twist ratio of 9.375 and wave widths of 13, 16, and 24 mm, respectively. This phenomenon can be attributed to the turbulence intensity generated by the corrugations on the

inserts, which results in rapid mixing of the flow and enhances heat transfer. It is observed that a reduction in wave width also increases the Nusselt number and the pressure drop.

In their study, Wang *et al.,* [16] examined the Nusselt number of tubes equipped with twisted tapes placed in the center under various widths. Their findings revealed that these tubes exhibited a 7–51% higher Nusselt number than plain tubes. Additionally, the performance of the tubes in the low Reynolds number region was found to be more effective than in the high Reynolds number. Heat transfer for round tubes with twisted tapes attached to the walls demonstrated superior performance compared to tubes with twisted tapes placed in the center. The increase in Nusselt number ranged from 3 to 18%. Furthermore, Sui *et al.,* [17] investigated wave-shaped microchannel heat sinks with rectangular cross-sections, which exhibited markedly superior heat transfer performance compared to straight microchannel heat sinks. In a separate study, Zhou *et al.,* [18] examined the heat transfer characteristics and flow resistance of heat sinks with zigzag microchannels and elucidated the correlation between heat transfer coefficients and flow resistance coefficients. Rahimi and Mehryar [19] demonstrated that axial heat conduction in channel walls, influenced by wall thermal conductivity and thickness, results in a decline in local Nusselt numbers at the inlet and also discrepancies in local Nusselt numbers at the outlet of the microchannel.

Wu *et al.,* [20] experimentally investigated tree-shaped microchannel heat sinks with four branch levels, achieving average surface temperatures ranging from 23.8 ◦C to 66.6 ◦C at heat flux ranging from 5 W/cm^2 to 8 W/cm^2. On the other hand, Qu and Mudawar [21] found that higher heat flux and Nusselt number were obtained near the inlet. An increase in Reynolds number increases the length of the developing region. Fully developed flow may not be achieved inside the heat sink for high Reynolds numbers. This results in increased heat transfer, but with the cost of increased pressure. Al Ketbi *et al.,* [22] conducted experiments that the Nusselt associated with spiral microchannels was higher than straight microchannels for a Reynolds range from 50 to 500. Moreira *et al.,* [23] conducted comparative experiments on heat transfer and pressure drop in converging and uniform microchannels, which showed that in single-row flow, converging microchannels performed better than uniform or diverging microchannels, especially at low flow rates. Dixit and Ghosh [24] investigated the Nusselt number and thermal resistance of diamond-shaped and rhombic-shaped microchannels and found that with increasing Reynolds number, the Nusselt number increased almost linearly and the thermal resistance decreased, while both were independent of heat flux. Harms *et al.,* [25] examined convective heat transfer of water in rectangular microchannels with widths of 251 µm and depths of 1000 µm. In the laminar regime with the Reynolds numbers studied, the measured local Nusselt numbers correspond well to classical developing flow theory. Furthermore, Abidin *et al.,* [26] stated that Design of Experiment (DOE) approach offers a significant improvement over the traditional One Factor at a Time (OFAT) method by providing more accurate predictions of optimal levels, leading to increased efficiency. Random experiments, on the other hand, often require numerous trials and are prone to errors due to limited or no statistical validation. DOE techniques, particularly Response Surface Methodology (RSM), are highly reliable as they achieve process or formulation goals with fewer experiments, thus reducing experimental time. Moreover, Azman *et al.,* [27] utilized the RSM for screening and optimizing processes by applying statistical and mathematical methods, enhancing the design's effectiveness.

In this study, Computational Fluid Dynamics (CFD) was employed to model a circular-shaped microchannel with an orifice-like obstruction in accordance with the ISO 5167:2003 standards. The impact of geometry configuration, Reynolds number, and wall heat flux on the Nusselt number and pressure drop was investigated. The results were subjected to further analysis using the Response Surface Method (RSM) in order to determine the most optimal combination between factors (geometry, Reynolds number, heat flux) and responses (Nusselt number and pressure drop).

2. Methodology

2.1 Microchannel

The microchannel has a diameter of 1 mm and a length of 100 mm. The orifice geometry was constructed in accordance with the ISO 5167:2003 standard. Figure 1 depicts the schematic of the microchannel, where T1-T8 represents the point where the local convective heat transfer will be analyzed. Moreover, Table 1 lists the details of eight (A-H) different geometry configurations. This study employed eight distinct microchannel configurations based on the position of the orifice. Where *X* represents the distance between inlet and the first orifice and *y* represents the distance between the orifices.

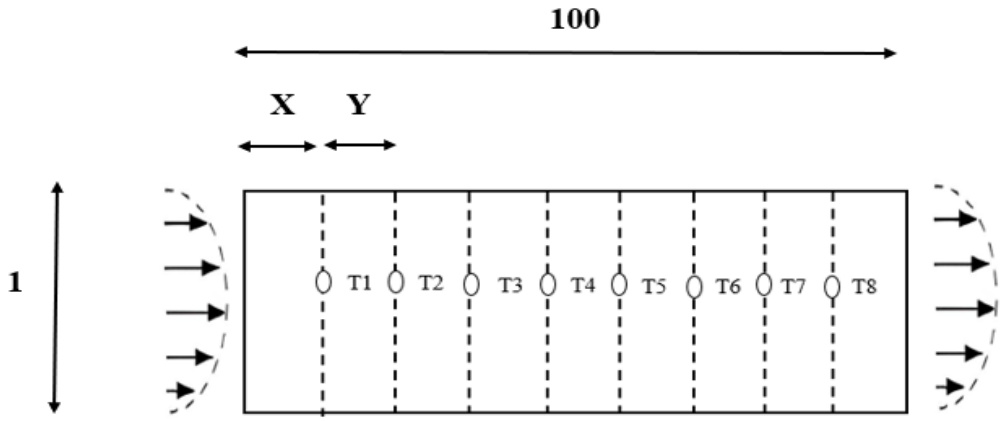

Fig. 1. Microchannel Design

Table 1
Description of Orifice Position on Microchannel

No.	Parameters	*X* (mm)	*Y* (mm)
1	A	0	0
2	B	25	25
3	C	30	30
4	D	10	20
5	E	20	20
6	F	30	20
7	G	12,5	12,5
8	H	15	15

Where:
X = Distance between Inlet and Orifice
Y = Distance between Orifices

2.2 Grid Independent Study on the Microchannel

A grid-independent study was conducted using five distinct mesh configurations. Element sizes of 50, 75, 100, 150, and 200 µm were investigated under identical boundary conditions. Additionally, Figure 2 illustrates the microchannel mesh.

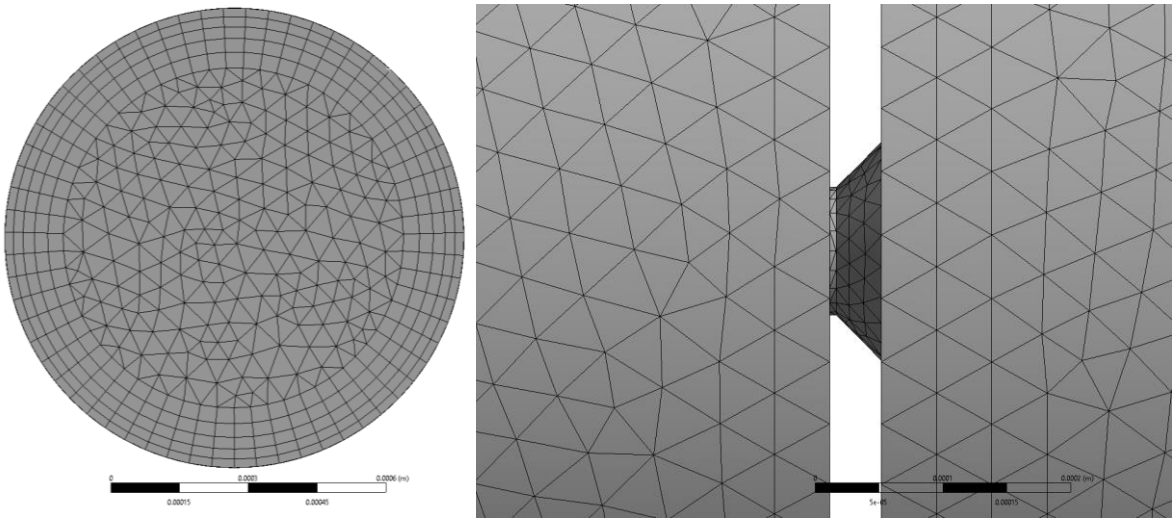

Fig. 2. Meshing on Microchannel

To perform the grid independent study, Figure 3 depicts the velocity profile across the channel diameter as a function of the element size. The outcome of the Grid Independence study shows that an element size of 50 µm with 2,640,128 elements is the optimal configuration for subsequent simulation. A 5% of velocity between element sizes 50 µm and 75 µm was observed compared to 8 % between 75 µm and 100 µm. Furthermore, this study employed two distinct wall heat fluxes of 5 W and 10 W as boundary conditions. Additionally, five distinct Reynolds numbers of 10, 30, 50, 70, and 90 were selected as the inlet condition.

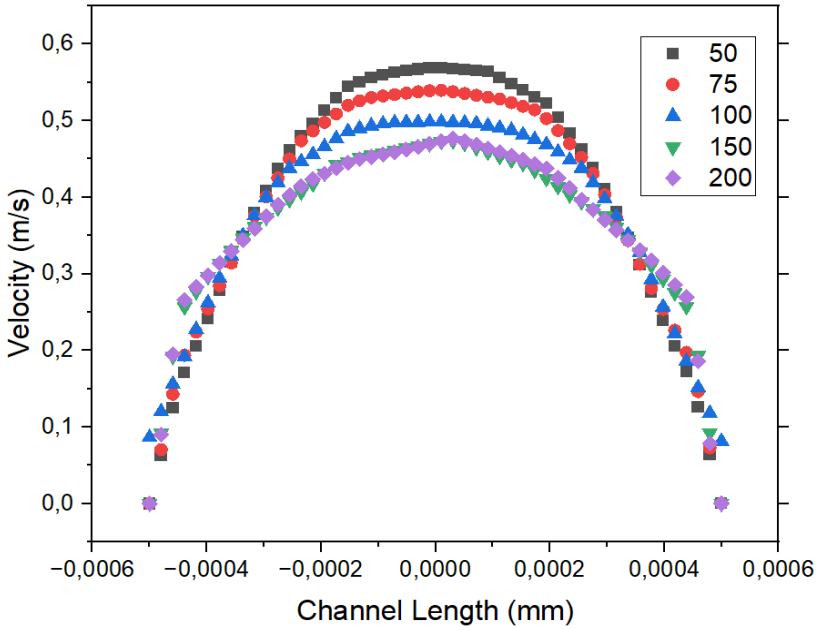

Fig. 3. Velocity profile of the microchannel over the channel diameter

2.3 Formulation of the Problem

Given that the flow is assumed to be two-dimensional and incompressible, the following governing Eq. (1) to Eq. (3) were employed to simulate the convective heat transfer in microchannels:

Conservation of mass:

$$\nabla \cdot \left(\rho \vec{V}\right) = 0 \tag{1}$$

Conservation of momentum:

$$\nabla \cdot \left(\rho \vec{V}\vec{V}\right) = -\nabla P + \nabla \cdot \left(\mu \nabla \vec{V}\right) \tag{2}$$

Energy equation:

$$\nabla \cdot \left(\rho \vec{V} c T\right) = \nabla \cdot (k \nabla T) \tag{3}$$

Where ρ, μ, and P are the density, dynamic viscosity, and pressure. Furthermore, the temperature, specific heat capacity, and thermal conductivity are written as T, c, and k, respectively.

Furthermore, the local heat transfer coefficient (h_x) was calculated using Eq. (4) as follows

$$h_x = \frac{q}{T_{w(x)} - T_{f(x)}} \tag{4}$$

The average heat transfer coefficient (h_{ave}) is further calculated using Eq. (5)

$$h_{ave} = \frac{1}{L}\int_o^L h_x dx \tag{5}$$

Moreover, the dimensionless average Nusselt (Nu_{ave}) number is calculated using Eq. (6)

$$Nu_{ave} = \frac{h_{ave} D}{k} \tag{6}$$

3. Results

3.1 Local Nusselt

Figure 4 depicts the local Nusselt number along the microchannel at a Reynolds number of 90 under eight distinct microchannel configurations (A to H). As illustrated, as the flow undergoes both hydrodynamic and thermal development, the area in close proximity to the inlet exhibits a higher Nusselt number for each geometry. Conversely, as the flow reaches a fully developed region, the Nusselt number declines and stabilizes. Moreover, over the channel length, several peaks of local Nusselt number were observed. The jump in Nusselt number can be associated with the position of the orifice, where the velocity increases as the cross-sectional area decreases.

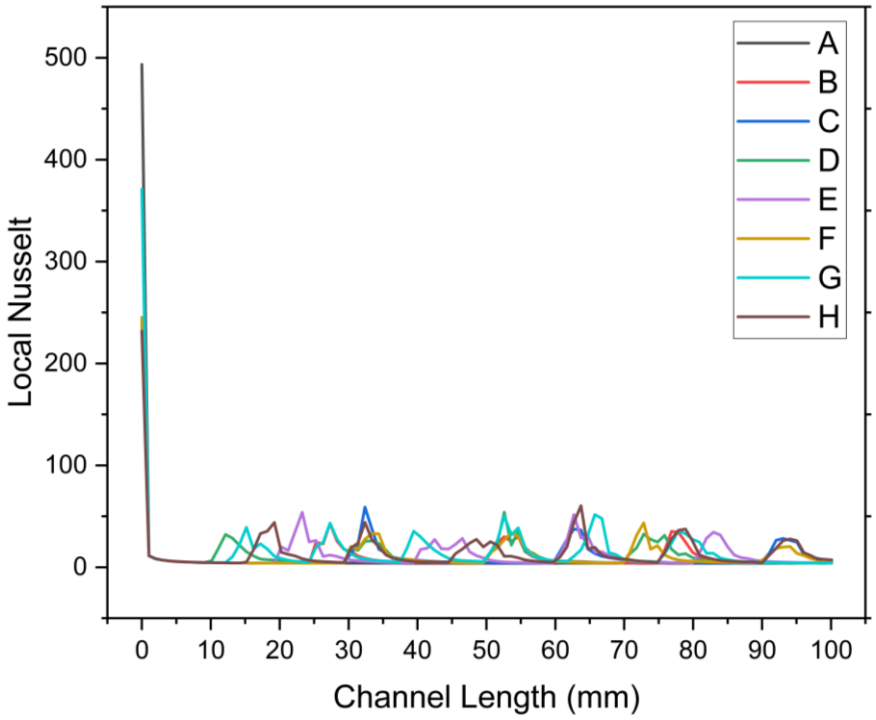

Fig. 4. Local Nusselt number under different microchannel configurations

3.2 Average Nusselt Number

Figure 5 depicts the average Nusselt number as a function of the Reynolds number for various geometry configurations. As illustrated, the Nusselt number increases with the Reynolds number. A notable increase is also evident with the introduction of an orifice into the microchannel. Geometry G at Reynolds number 90 exhibits an 89% increase in Nusselt compared to geometry A (basic geometry). The abrupt alteration in microchannel diameter resulting from the presence of an orifice can be attributed to the observed increase in Nusselt number. Previous research by Sanei and Ayani [28] indicated that an increase in Reynolds number is associated with elevated velocity. A higher Reynolds number leads to an enhancement in the Nusselt number and, consequently, an improvement in convective heat transfer.

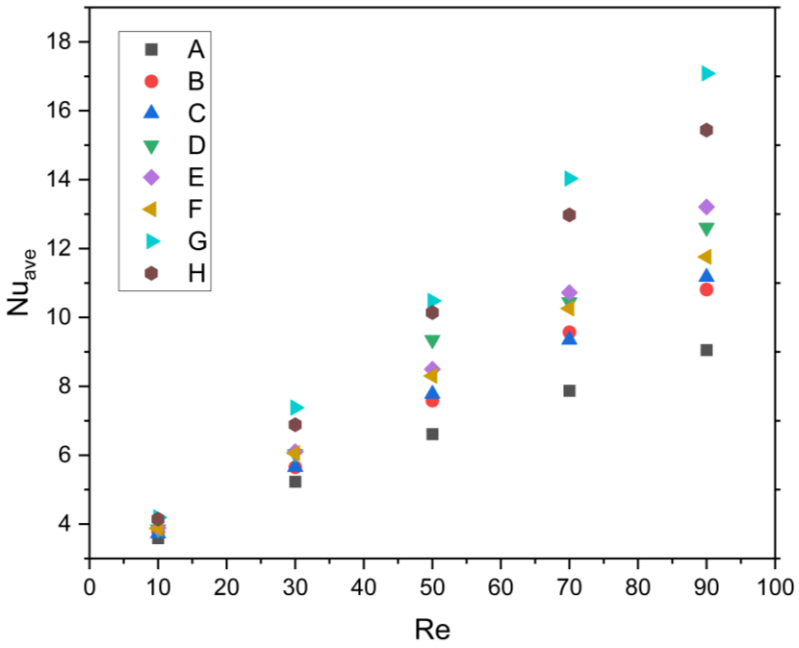

Fig. 5. Average Nusselt number vs Reynolds number under different microchannel configurations

3.3 Pressure Drop

Figure 6 illustrates that the microchannel without an orifice, with three orifices, four orifices, and six orifices exhibits notable variations in several key parameters. At a Reynolds number of 90, Geometry G exhibited a 190.54% increase in pressure drop compared to Geometry B. Similarly, at a Reynolds number of 90, Geometry G exhibited a 67.21% increase in pressure drop compared to Geometry C. A 96.97% increase in pressure drop is observed when comparing Geometry D to Geometry G at Reynolds number 90. A 131.44% increase in pressure drop is observed when comparing Geometry E to Geometry G at Reynolds number 90. Finally, a 99% increase in pressure drop is observed when comparing Geometry G at Reynolds number 90 to Geometry F. A 1.77% increase in pressure drop was observed when comparing Geometry F to Geometry G at Reynolds number 90. In contrast, a 166.72% increase in pressure drop was observed when comparing Geometry H to Geometry G at Reynolds number 90.

The observed increase in pressure drop can be attributed to an increase in the Reynolds number and the distance between the inlet and the orifice. As the Reynolds number increases, the inertia force in the fluid flow also rises, resulting in a corresponding increase in pressure drop. Furthermore, an expansion in the distance between the inlet and the orifice leads to a heightened resistance in the fluid flow, which contributes to the elevated pressure drop. Consequently, the higher the Reynolds number and the distance between the inlet and the orifice, the more pronounced the percentage increase in pressure drop (Δp).

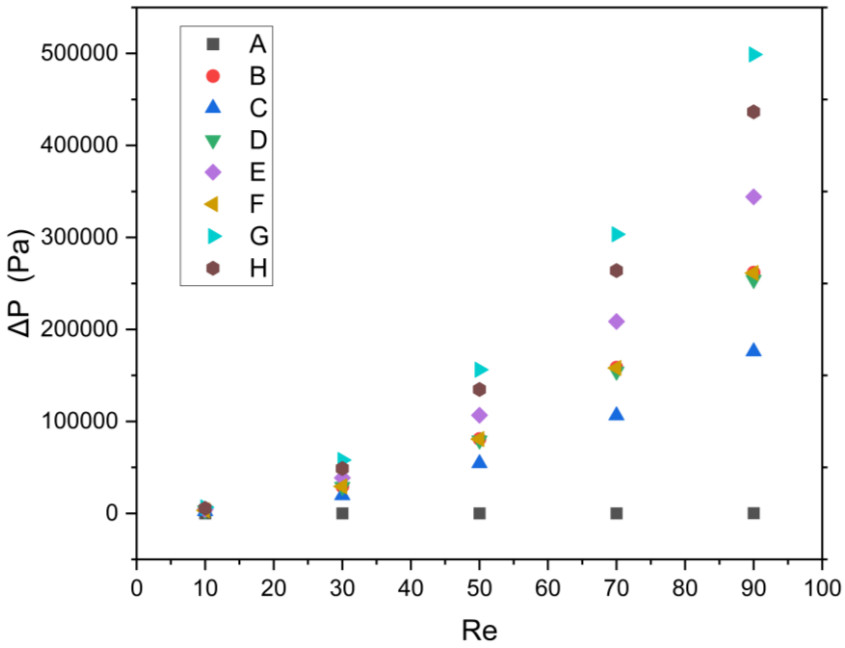

Fig. 6. Pressure drop vs Reynolds number number under different microchannel configurations

Figure 7 shows the velocity contour as the fluid flows through the orifice at a distance of 15 mm from the inlet when the Reynolds number is equal to 90. As can be seen, the velocity increases and reaches the maximum value at the orifice. The change in flow behavior changes the steadiness of the flow. Thus, the flow re-enters the developing stage of hydrodynamics. The sudden increase in velocity can be accounted as the source of increase in pressure drop.

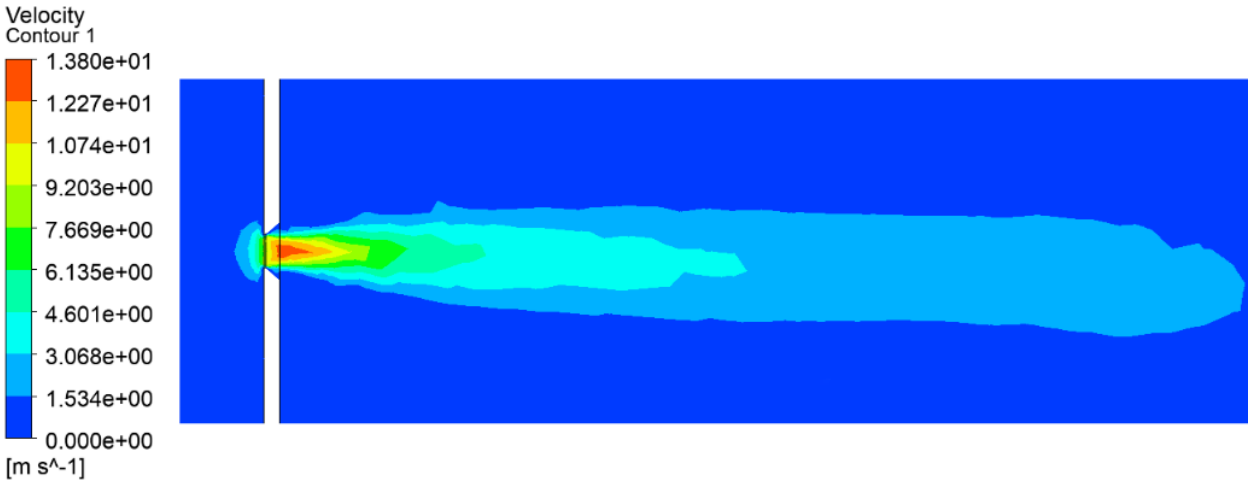

Fig. 7. Velocity contour around the orifice at Re = 90

3.4 Data from Response Surface Methodology

The testing was conducted using Design Expert software, where the Response Surface Methodology results for various microchannel geometries were obtained by utilizing other data such as Reynolds numbers of 10, 30, 50, 70, 90, heat flux (q), and the number of orifices.

The fit statistics in Table 2 demonstrate a slightly superior result when measured by R^2, using the optimal lambda values based on the Box-Cox Plot. The study proceeded with lambda values for pressure drop and Nusselt average being 0.12 and 1.03, respectively. A higher R^2 implies that the

independent variable can account for a significant portion of the observed differences in the dependent variable. Adequate precision on both responses in the transformed version also shows a higher value, which can be interpreted as higher accuracy in the estimation obtained from the statistical model or analysis. This indicates that the findings are sufficiently precise to permit the drawing of meaningful conclusions.

Table 2
Fit statistics for pressure drop and average Nusselt number

Response	Pressure drop (R_1)	Nusselt Average (R_2)
Std. Dev.	33513.36	0.6899
Mean	1.140E+05	8.38
C.V. %	29.39	8.23
R^2	0.9436	0.9678
Adjusted R^2	0.9315	0.9609
Predicted R^2	0.9168	0.9534
Adeq Precision	30.4210	40.8698

The interaction between Factor A and Factor B is proposed as a two-factor interaction for both responses. Subsequently, an ANOVA was conducted to ascertain the significance of parameters. This analysis revealed that all parameters and their interactions are significant (p-value < α, where α is 0.05), with the exception of factor AB in the average Nusselt number in Table 3. This indicates that the interaction between the distance between the inlet and orifice and the Reynolds number is not significantly related to the average Nusselt number.

Table 3
ANOVA for pressure drop and average Nusselt number

Response	Model	Source	Sum of Squares	df	Mean Square	F-value	P-value
R_1 Pressure drop (0.12)	Quartic	Model	1.221E+12	14	8.724E+10	77.68	< 0.0001
		A-Distance between Inlet and Orifice	2.826E+09	1	2.826E+09	2.52	0.1175
		B-Reynolds number	1.441E+11	1	1.441E+11	128.26	< 0.0001
		AB	9.600E+07	1	9.600E+07	0.0855	0.7709
		Residual	7.300E+10	65	1.123E+09		
		Lack of Fit	6.228E+10	20	3.114E+09	13.07	< 0.0001
		Pure Error	1.072E+10	45	2.383E+08		
R_2 Nusselt Average (1.03)	Quartic	Model	929.43	14	66.39	139.50	< 0.0001
		A-Distance between Inlet and Orifice	0.0563	1	0.0563	0.1183	0.7320
		B-Reynolds number	112.26	1	112.26	235.90	< 0.0001
		AB	1.63	1	1.63	3.42	0.0689
		Residual	30.93	65	0.4759		

Lack of Fit	29.30	20	1.47	40.41	< 0.0001
Pure Error	1.63	45	0.0363		
Cor Total	960.36	79			

Regression equations were obtained in Eq. (7) and Eq. (8)

$$R_1^{0.12} = 144948.37 + 38878.10A + 197357.38B - 10176.63AB \quad (7)$$

$$R_2^{1.03} = 10.18 - 0.1735A + 5.5094B - 1.3254AB \quad (8)$$

The two responses are pressure drop (R_1) and Nusselt average (R_2), while the two factors are the distance between the inlet and orifice (A) and Reynolds number (B). Variable AB represents the interaction of both factors. To obtain Variable AB, a regression analysis or factorial design experiment was performed to see how changes in one factor affect the response while the other factors also change. If AB shows a positive effect, it means that the interaction between the two factors increases the response. Conversely, if AB shows a negative effect, it means that the interaction between the two factors decreases the response. The exponents on both functions are transformations based on the suggested lambda. All variables, including the distance between the inlet and orifice and the Reynolds number, as well as their interaction, demonstrate a positive correlation with pressure drop raised to the power of 0.12 in Eq. (7). The coefficients of each factor's variables illustrate the extent to which they influence the corresponding response. With regard to the square of the Nusselt average in Eq. (8), the Reynolds number is the sole factor that exerts a positive influence. Conversely, the distance between the inlet and orifice, in conjunction with the interaction between the two factors (Factor AB), exerts an inverse influence. This implies that as the distance between the inlet and orifice and the interaction of both factors increase, the value of the average Nusselt number will decline.

If the residuals follow a normal distribution, it can be determined using the normal probability plot (straight line). In Figure 8, the value range for pressure drop is 22.9325–498938 Pa, while for Nusselt average is 3.59403–17.0844. There are some data points that deviate from the normal line, which will be validated further in the next diagnosis.

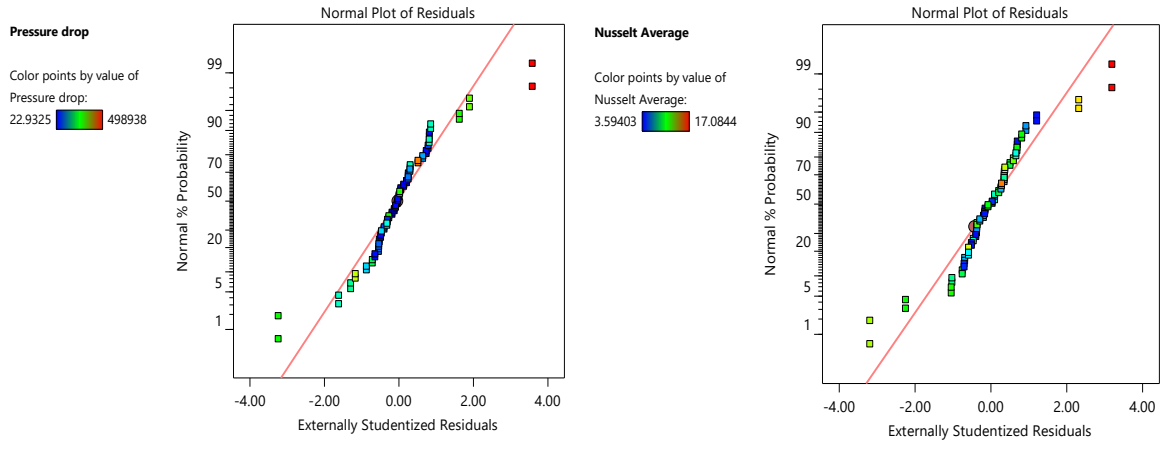

(a) (b)

Fig. 8. Normal plot for (a) pressure drop and (b) average Nusselt number

The plot between residuals and predicted response values should exhibit a random scatter, with a constant residual range across the graph. The data points on the graph are randomly distributed. Figure 9 indicates that the plot of residuals versus experimental run-order searches for hidden

variables that may have influenced the response during the experiment. The plot tends to display a random scatter. The plot of residuals versus any factor checks whether the variance not explained by the model differs for different levels of a factor. The plot demonstrates a random scatter. The predicted versus actual plot implies that both responses show a strong fit between predicted and actual values.

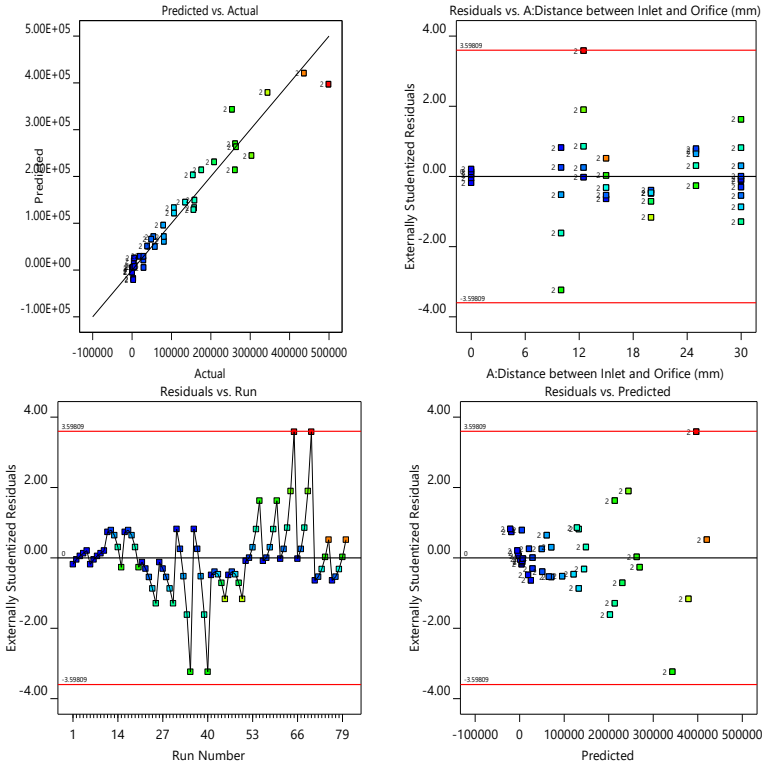

(a)

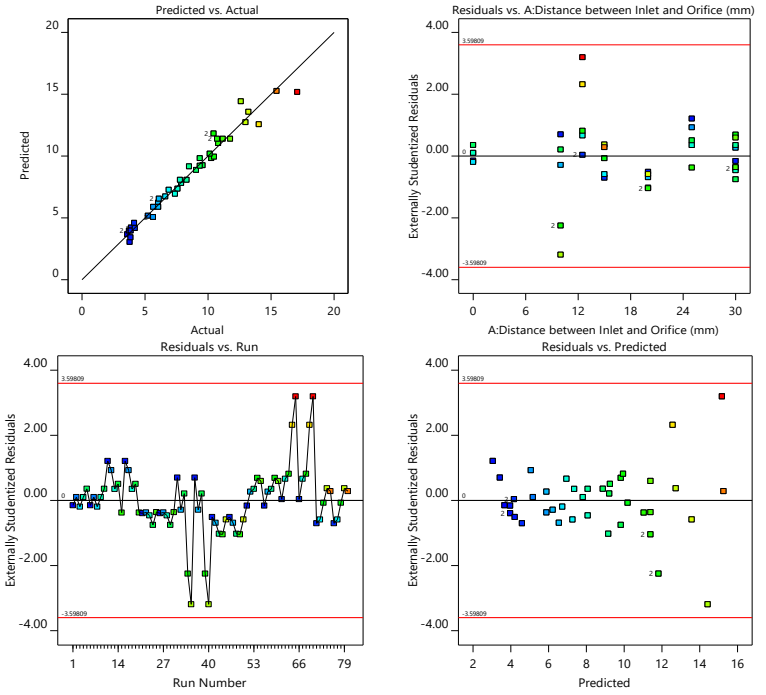

(b)

Fig. 9. Diagnostics of residuals, predicted, run, and actual of (a) pressure drop and (b) average Nusselt number

The graph evaluates the interaction between the two factors and the response. The perturbation plot compares the effects of all factors at a specific point. The response is plotted while holding other factors constant. The slope indicates the sensitivity of the response to the corresponding factor. For pressure drop in Figure 10(a), the distance between the inlet and orifice shows a higher sensitivity compared to the Reynolds number. In contrast, the Reynolds number demonstrates a high degree of sensitivity to the Nusselt average, whereas the distance between the inlet and orifice exhibits a similar tendency but with an inverse effect. The factor of interaction AB of the black line in Figure 10(b) represents the lower limit, while the red line represents the upper limit. When discussing pressure drop, the upper limit is located above the lower limit, while this is the same for the Nusselt average. This indicates that pressure drop will increase with the factor interaction, whereas the average Nusselt number will decline.

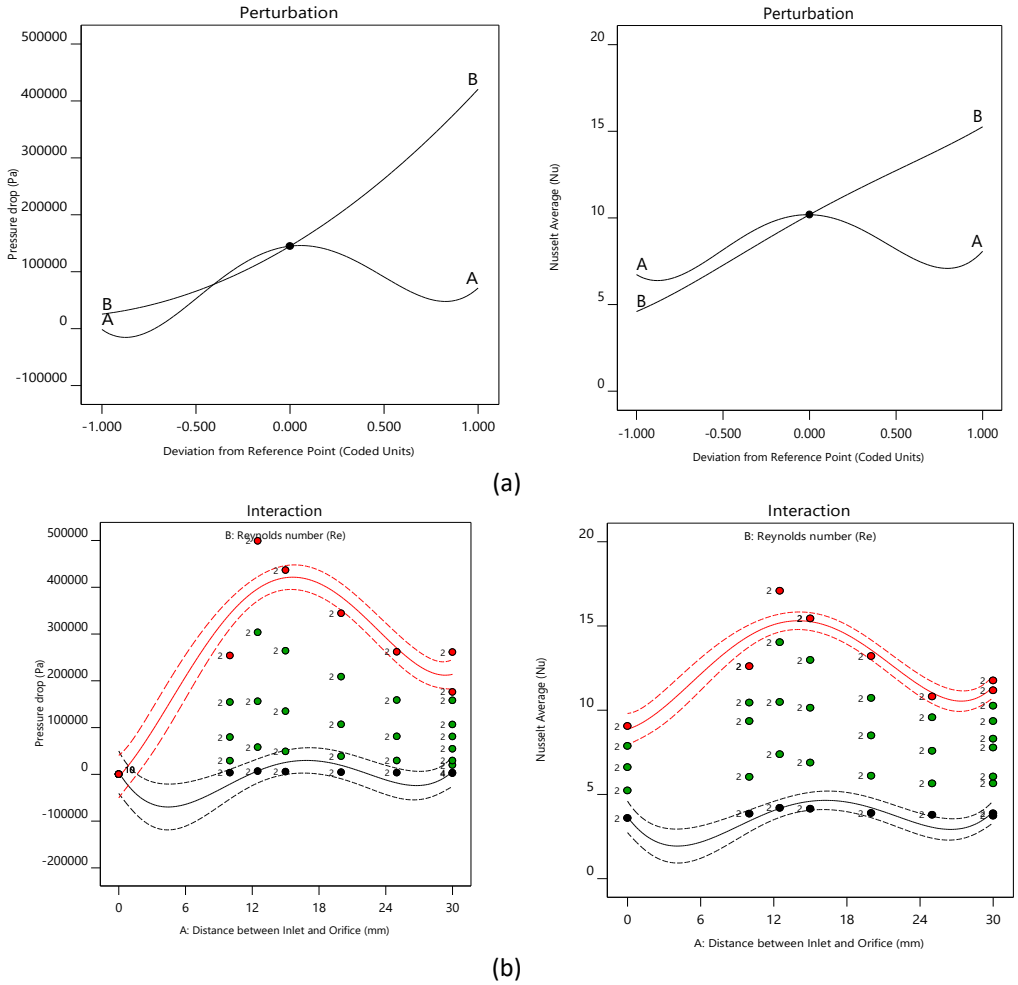

Fig. 10. Model graph for (a) perturbation and (b) factor interaction of pressure drop and average Nusselt number

In Figure 11 and Figure 12, contour and 3D surface graphs plot both factors on the x and y axes, while the corresponding response as a dependent variable on the z-axis is visualized. The colors indicate the range of responses for easier analysis. On the 3D surface in Figure 12, the wavy plot shows the two-factor interaction model between factors for each response. Figure 11(a) and Figure 11(a) plot the pressure drop response, which is aimed to be minimized. Thus, the desired area is located at the top left in blue. The Nusselt average response, plotted in Figure 10(b) and Figure 11(b), is aimed to be maximized. Therefore, the desired area is located at the top right in red.

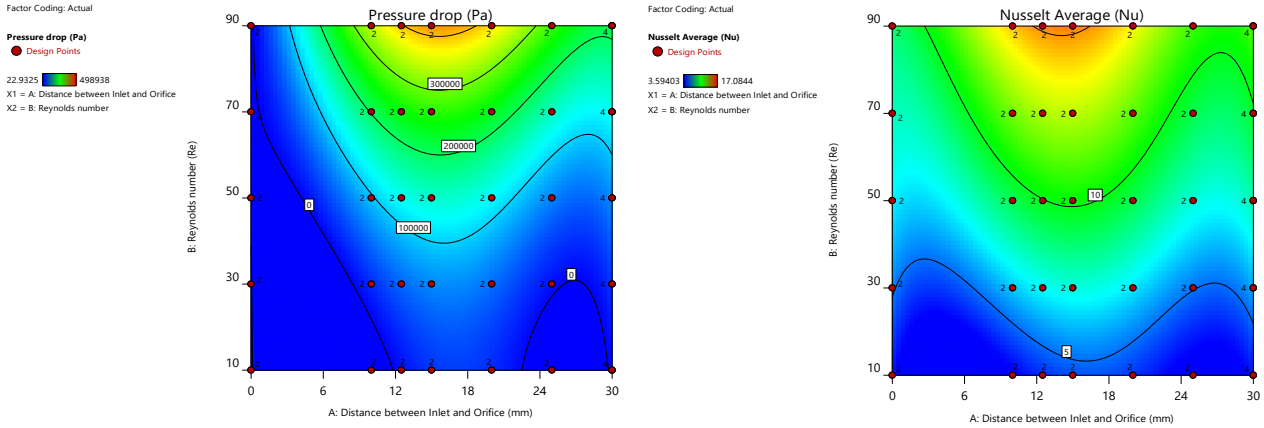

(a) (b)

Fig. 11. Contour of (a) pressure drop and (b) average Nusselt number

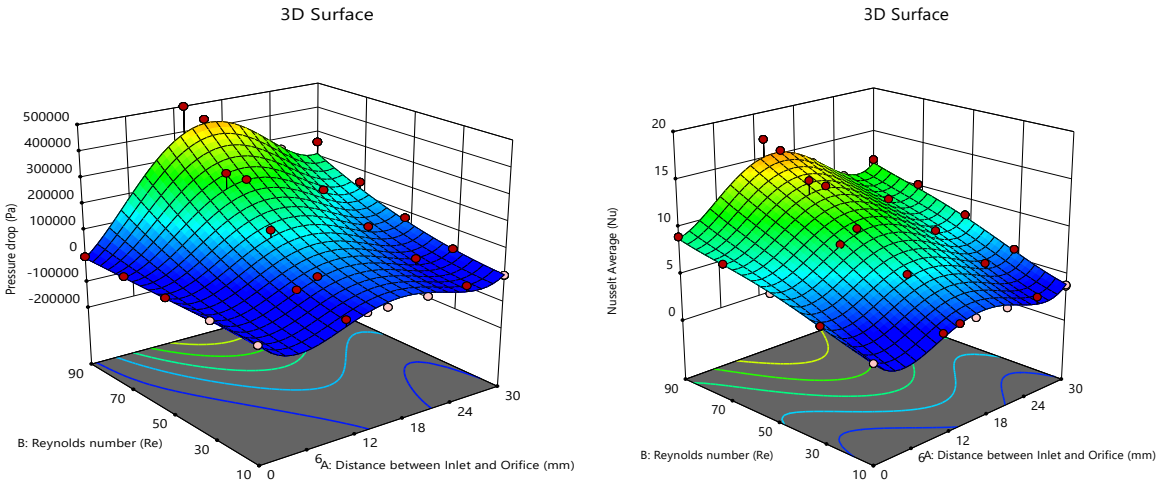

(a) (b)

Fig. 12. 3D Surface of (a) pressure drop and (b) average Nusselt number

3.5 Response Surface Methodology Optimization

Once the mathematical model has been formulated, optimization methods are employed to determine the optimal conditions for the system. The objective is to discover the combination of input factors that enhances or reduces the desired responses. Numerical optimization was conducted using the same software by setting the boundary range for all parameters. The range displayed in Figure 13 was utilized fully due to the limited data. Through trial and error, this range also demonstrated an excellent desirability rating in the solutions. The optimization constraints are presented in Table 4.

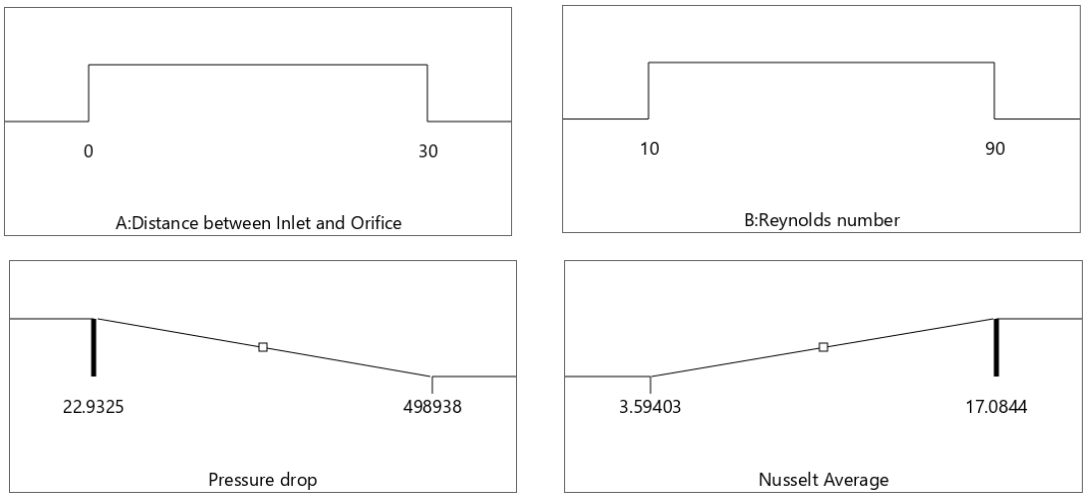

Fig. 13. Numerical criteria for RSM optimization

Table 4
Constraints of Response Surface Methodology Optimization

Variables	Goal	Lower limit	Upper limit
Distance between Inlet and Orifice	is in range	0	30
Reynolds number	is in range	10	90
Pressure drop	minimize	22.9325	498938
Nusselt Average	maximize	3.59403	17.0844

The number of solutions and the solutions resulting from the optimization were also compared. It should be noted that the objective is to minimize pressure drop and maximize the Nusselt average. The desirability algorithm is based on mathematical functions that measure the degree of alignment between the actual value and the predefined target ranges. The desirability value reflects the proximity of the actual response value to the target value or range. Following the boundary setup, the RSM numerical optimization procedure yielded 14 potential solutions, with desirability serving as a measure of optimization performance. The higher the desirability, the more optimal the solution. Desirability values in Table 5 range from 0.584 to 0.631. Based on the aforementioned suggestion, option number 1 was selected as the most optimal solution. This option was selected based on a distance between the inlet and orifice of 2.831 mm and a Reynolds number of 90, resulting in a pressure drop of 86089.542 Pa and a Nusselt average of 10.079. This solution is based on the predictive model, which employs a regression equation.

Table 5
Solutions of Response Surface Methodology Optimization

No.	Factors		Responses		Desirability
	A: Distance between Inlet and Orifice (mm)	B: Reynolds number	Pressure drop (Pa)	Nusselt Average	
1	2.831	90.000	86089.542	10.079	0.631
2	2.944	90.000	90290.959	10.146	0.631
3	2.722	90.000	82054.621	10.016	0.631
4	2.579	90.000	76796.851	9.934	0.631
5	2.260	90.000	65273.820	9.759	0.630
6	3.371	90.000	106465.601	10.405	0.630
7	3.482	90.000	110690.886	10.474	0.630
8	1.929	90.000	53653.963	9.588	0.630
9	1.719	90.000	46440.568	9.485	0.629
10	3.849	90.000	124871.285	10.707	0.629

11	1.000	90.000	23182.507	9.175	0.628
12	0.684	90.000	13708.076	9.062	0.628
13	0.543	90.000	9662.330	9.017	0.628
14	30.000	75.944	155032.034	10.274	0.584

The relationship between the generated solutions and both variables is depicted in Figure 10. It is preferable to select solutions with high desirability, indicated by the area of selected solutions being in the top-left. This indicates that high performance is achieved with approximately the leftmost value of the Distance between the Inlet and Orifice range and a high Reynolds number, as seen in Figure 14(a). The trade-off between the two responses is depicted by the contours in the pressure drop variable in Figure 14(b), where the desired area is located in the top-left corner, and the Nusselt average variable in Figure 14(c), where the desired area is also in the top-left corner.

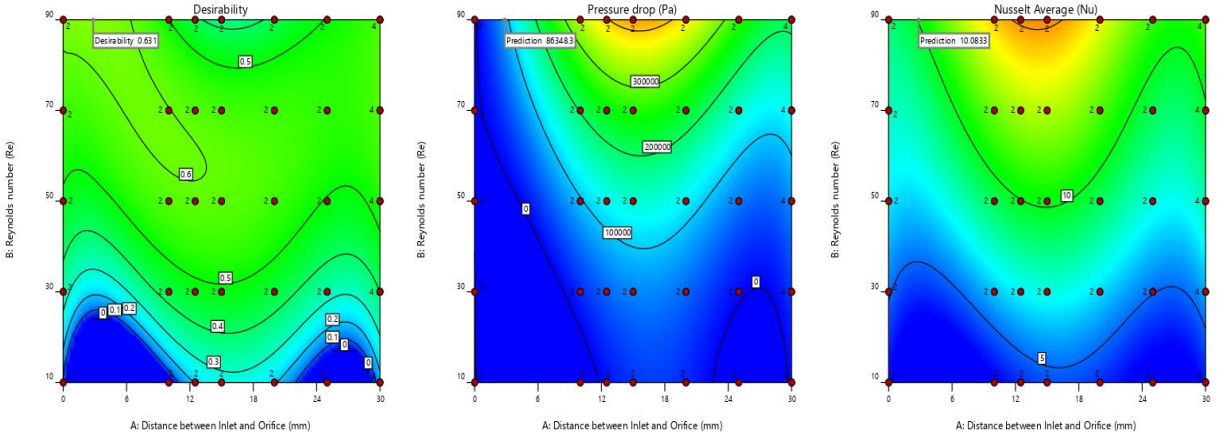

(a) (b) (c)

Fig. 14. Contour of Response Surface Methodology (RSM) solutions (a) desirability, (b) pressure drop, and (c) The Average Nusselt number

4. Conclusions

Based on the experiments, data, and analysis conducted, several conclusions can be drawn as follows:

i. Based on the pressure drop data, a significant increase in pressure drop (Δp) is observed with increasing values of the distance between the inlet and orifice and the Reynolds number.
ii. The Nusselt average data indicates an increase in the percentage change of the Nusselt average with increasing values of the distance between the inlet and orifice and the Reynolds number.
iii. The analysis results indicate that factors such as the Reynolds number and the distance between the inlet and orifice significantly influence the system performance, particularly in pressure drop and Nusselt average. Optimizing these factors can result in a more efficient and optimal design.
iv. Anova Response Surface Methodology demonstrates the significance of the model used in statistical analysis. The optimization process revealed that a microchannel with a Reynolds number of 90 and a distance between the inlet and orifice of 2.83238 mm is a promising solution.

In conclusion, data analysis indicates that parameters such as the distance between the inlet and orifice, Reynolds number, and heat flux have a significant impact on microchannel performance. Optimization of these parameters can result in a more efficient and optimal design.

Acknowledgment
The financial support from Ministry of Education, Culture, Research, and Technology of Republic of Indonesia through Master Thesis Research Grant with contract number NKB-955/UN2.RST/HKP.05.00/2024 is truly acknowledged.

References

[1] Ohadi, Michael, Kyosung Choo, Serguei Dessiatoun, and Edvin Cetegen. *Next generation microchannel heat exchangers*. New York: Springer, 2013. https://doi.org/10.1007/978-1-4614-0779-9
[2] Kwon, Dohoon, Lingxue Jin, WooSeok Jung, and Sangkwon Jeong. "Experimental investigation of heat transfer coefficient of mini-channel PCHE (printed circuit heat exchanger)." *Cryogenics* 92 (2018): 41-49. https://doi.org/10.1016/j.cryogenics.2018.03.011
[3] Khan, Mesbah G., and Amir Fartaj. "A review on microchannel heat exchangers and potential applications." *International Journal of Energy Research* 35, no. 7 (2011): 553-582. https://doi.org/10.1002/er.1720
[4] Wu, Peiyi, and W. A. Little. "Measurement of the heat transfer characteristics of gas flow in fine channel heat exchangers used for microminiature refrigerators." *Cryogenics* 24, no. 8 (1984): 415-420. https://doi.org/10.1016/0011-2275(84)90015-8
[5] Dehghan, Maziar, Mahdi Daneshipour, Mohammad Sadegh Valipour, Roohollah Rafee, and Seyfolah Saedodin. "Enhancing heat transfer in microchannel heat sinks using converging flow passages." *Energy Conversion and Management* 92 (2015): 244-250. https://doi.org/10.1016/j.enconman.2014.12.063
[6] Kose, Haluk Anil, Alperen Yildizeli, and Sertac Cadirci. "Parametric study and optimization of microchannel heat sinks with various shapes." *Applied Thermal Engineering* 211 (2022): 118368. https://doi.org/10.1016/j.applthermaleng.2022.118368
[7] Wang, Hongtao, Zhihua Chen, and Jianguo Gao. "Influence of geometric parameters on flow and heat transfer performance of micro-channel heat sinks." *Applied Thermal Engineering* 107 (2016): 870-879. https://doi.org/10.1016/j.applthermaleng.2016.07.039
[8] Kim, Byongjoo. "An experimental study on fully developed laminar flow and heat transfer in rectangular microchannels." *International Journal of Heat and Fluid Flow* 62 (2016): 224-232. https://doi.org/10.1016/j.ijheatfluidflow.2016.10.007
[9] Murugesan, P., K. Mayilsamy, and S. Suresh. "Turbulent heat transfer and pressure drop in tube fitted with square-cut twisted tape." *Chinese Journal of Chemical Engineering* 18, no. 4 (2010): 609-617. https://doi.org/10.1016/S1004-9541(10)60264-9
[10] He, Yan, Li Liu, Pengxiao Li, and Lianxiang Ma. "Experimental study on heat transfer enhancement characteristics of tube with cross hollow twisted tape inserts." *Applied Thermal Engineering* 131 (2018): 743-749. https://doi.org/10.1016/j.applthermaleng.2017.12.029
[11] Ali, Abdullah Masoud, Aldo Rona, Hakim T. Kadhim, Matteo Angelino, and Shian Gao. "Thermo-hydraulic performance of a circular microchannel heat sink using swirl flow and nanofluid." *Applied Thermal Engineering* 191 (2021): 116817. https://doi.org/10.1016/j.applthermaleng.2021.116817
[12] Song, Ying-Qing, Niloufar Izadpanahi, Mohammad Ali Fazilati, Yu-Pei Lv, and Davood Toghraie. "Numerical analysis of flow and heat transfer in an elliptical duct fitted with two rotating twisted tapes." *International Communications in Heat and Mass Transfer* 125 (2021): 105328. https://doi.org/10.1016/j.icheatmasstransfer.2021.105328
[13] Eiamsa-Ard, Smith, Kwanchai Nanan, Khwanchit Wongcharee, Kittisak Yongsiri, and Chinaruk Thianpong. "Thermohydraulic performance of heat exchanger tube equipped with single-, double-, and triple-helical twisted tapes." *Chemical Engineering Communications* 202, no. 5 (2015): 606-615. https://doi.org/10.1080/00986445.2013.858038
[14] Vinoth, R., B. Sachuthananthan, A. Vadivel, S. Balakrishnan, and A. Gnana Sagaya Raj. "Heat transfer enhancement in oblique finned curved microchannel using hybrid nanofluid." *International Journal of Thermal Sciences* 183 (2023): 107848. https://doi.org/10.1016/j.ijthermalsci.2022.107848
[15] Dhamane, N. B., D. B. Nalawade, and M. M. Dange. "Performance analysis of wavy twisted tape insert for heat transfer in a circular tube." *International Journal for Technological Research in Engineering* 1, no. 6 (2014).

[16] Wang, Li, Peiyong Ni, and Guannan Xi. "The effect of off-center placement of twisted tape on flow and heat transfer characteristics in a circular tube." *Scientific Reports* 11, no. 1 (2021): 6844. https://doi.org/10.1038/s41598-021-86285-0
[17] Sui, Y., P. S. Lee, and C. J. Teo. "An experimental study of flow friction and heat transfer in wavy microchannels with rectangular cross section." *International Journal of Thermal Sciences* 50, no. 12 (2011): 2473-2482. https://doi.org/10.1016/j.ijthermalsci.2011.06.017
[18] Zhou, Xiang, Chen Zeng, Yinxi Song, Ming Jiao, Feixi Zhang, and Maolong Liu. "Experimental study on heat transfer and flow resistance performance of a microchannel heat exchanger with zigzag flow channels." *Progress in Nuclear Energy* 147 (2022): 104190. https://doi.org/10.1016/j.pnucene.2022.104190
[19] Rahimi, Mohammad, and Reza Mehryar. "Numerical study of axial heat conduction effects on the local Nusselt number at the entrance and ending regions of a circular microchannel." *International Journal of Thermal Sciences* 59 (2012): 87-94. https://doi.org/10.1016/j.ijthermalsci.2012.04.017
[20] Wu, Shaojie, Kai Zhang, Ge Song, Jinchen Zhu, and Bingru Yao. "Experimental study on the performance of a tree-shaped mini-channel liquid cooling heat sink." *Case Studies in Thermal Engineering* 30 (2022): 101780. https://doi.org/10.1016/j.csite.2022.101780
[21] Qu, Weilin, and Issam Mudawar. "Analysis of three-dimensional heat transfer in micro-channel heat sinks." *International Journal of Heat and Mass Transfer* 45, no. 19 (2002): 3973-3985. https://doi.org/10.1016/S0017-9310(02)00101-1
[22] Al Ketbi, Shamsa, Amna Al Rashdi, Sabah Al Haddad, Salini Krishnan, and Bobby Mathew. "Simulation based investigation of Nusselt number and Poiseuille number in helical microchannels." *International Journal of Thermofluids* 21 (2024): 100532. https://doi.org/10.1016/j.ijft.2023.100532
[23] Moreira, Debora C., Gherhardt Ribatski, and Satish G. Kandlikar. "Heat transfer and pressure drop in single-phase flows in tapered microchannels." *Journal of Heat Transfer* 144, no. 7 (2022): 072502. https://doi.org/10.1115/1.4054351
[24] Dixit, Tisha, and Indranil Ghosh. "Low Reynolds number thermo-hydraulic characterization of offset and diamond minichannel metal heat sinks." *Experimental Thermal and Fluid Science* 51 (2013): 227-238. https://doi.org/10.1016/j.expthermflusci.2013.08.002
[25] Harms, Todd M., Michael J. Kazmierczak, and Frank M. Gerner. "Developing convective heat transfer in deep rectangular microchannels." *International Journal of Heat and Fluid Flow* 20, no. 2 (1999): 149-157. https://doi.org/10.1016/S0142-727X(98)10055-3
[26] Abidin, Muhamad Hissammuddin Shah Zainal, Umi Aisah Asli, Nor Dina Sakaria, Nur Raudhah Azman, and Aishah Abdul Jalil. "Application of Response Surface Methodology in the Formulation of an Eco-friendly Degreaser using Rhamnolipid Biosurfactant." *Journal of Advanced Research in Applied Sciences and Engineering Technology* 46, no. 1 (2024): 118-135. https://doi.org/10.37934/araset.46.1.118135
[27] Azman, Azraf, Mohd Zamri Yusoff, Azfarizal Mukhtar, Prem Gunnasegaran, Ng Khai Ching, and Ahmad Shah Hizam Md Yasir. "Application of box-behnken design with response surface methodology to analyse friction characteristics for corrugated pipe via CFD." *CFD Letters* 15, no. 7 (2023): 1-13. https://doi.org/10.37934/cfdl.15.7.113
[28] Sanei, Hamed, and Mohammad Bagher Ayani. "Numerical Investigation of the Effect of Geometrical Shape of Plate Heat Exchangers on Heat Transfer Efficiency." *International Journal of Mechanical and Mechatronics Engineering* 10, no. 5 (2016): 879-883.